

Supporting Information

FABRICATION, THERMAL ANALYSIS, AND HEAVY ION IRRADIATION RESISTANCE OF EPOXY MATRIX NANOCOMPOSITES LOADED WITH SILANE-FUNCTIONALIZED CERIA NANOPARTICLES

Clare Davis-Wheeler Chin[†], Marissa A. Ringgold[†], Erica M. Redline[§], Avi G. Bregman[†],
Amanda S. Peretti[§], Khalid Hattar[§], and LaRico J. Treadwell^{†*}

[†]Advanced Materials Laboratory, Sandia National Laboratories
1001 University Blvd. SE, Suite 100, Albuquerque, NM USA

[§]Sandia National Laboratories, P.O. Box 5800, Albuquerque, NM 87185-1411, USA

Please address all correspondence to Dr. LaRico J. Treadwell
Email: ljtread@sandia.gov; Tel.: (505) 389-3503; Fax: (505) 284-3017

TABLE OF CONTENTS

Table S1	SRIM simulation inputs for neat epoxy and composites	S2
Figure S1	FTIR spectra for pristine ceria and SCA-NPs	S3
Table S2	Vibrational data for pristine ceria and SCA-NPs	S3
Figure S2	TGA weight loss and derivative weight change curves for SCA-NPs	S4
Table S3	TGA percent weight loss of SCA-NPs	S4
Figure S3	Derivative weight change curves of composites	S5
Table S4	Decomposition rate of composites at DWC maximum temperature	S5
Figure S4	DSC curves showing T_g variation with nanofiller loading	S6
Table S5	Glass transition temperature values	S6
Figure S5	Surface SEM for MTES composites before and after irradiation	S7
Figure S6	Cross-sectional SEM images for MTES composites before and after irradiation	S8
Scheme S1	Initiation of radical degradation in epoxy aliphatic segment	S9
Scheme S2	Initiation of radical degradation in bisphenol A (BPA) moiety	S10
Scheme S3	Degradation of BPA moiety via Radical K reactions	S10

	<u>H</u>	<u>C</u>	<u>O</u>	<u>Ce</u>
<u>Energy values (eV)</u>				
Displacement	2.0	7.4	2.0	4.2
Surface binding	10	28	28	56
Lattice binding	0	0	0	0
<u>Atom stoichiometry</u>				
Neat epoxy	19	18	3	0
Ce20	15.2	14.4	2.8	0.2
Ce60	7.6	7.2	2.4	0.6

Table S1. Summary of input and calculation parameters for SRIM simulations

Binding energy values were supplied by the SRIM program. Displacement energy represents the energy needed for a recoil to overcome lattice forces and move at least one atom spacing away from its original site, whereas lattice binding energy is the energy lost by every target atom leaving its original lattice site and recoiling within the target.

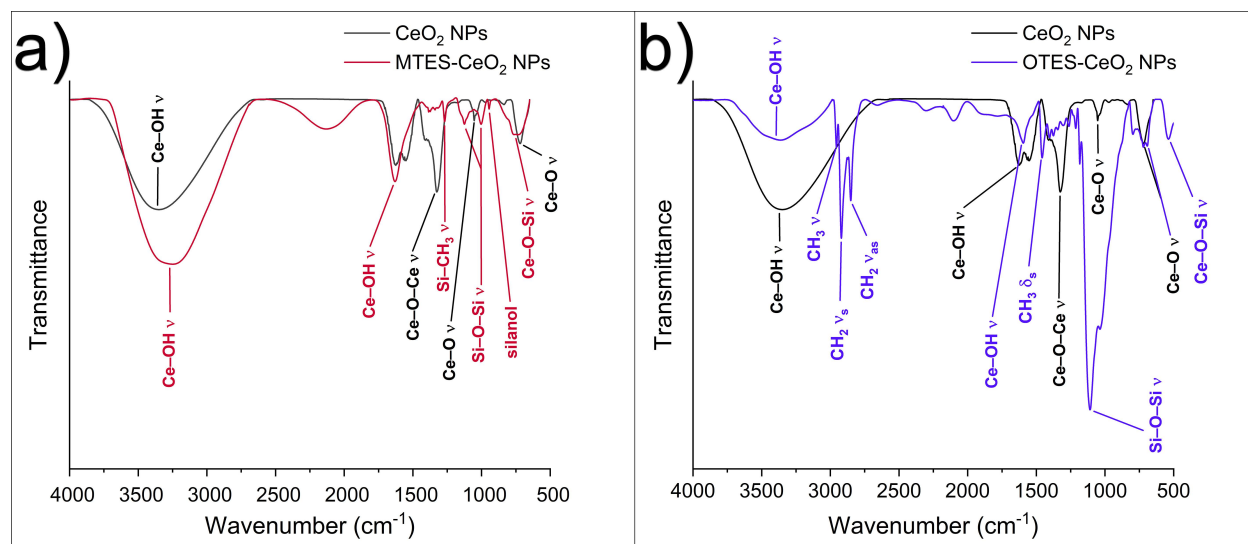


Figure S1. FTIR spectra of pristine ceria NPs compared to SCA-NPs functionalized with (a) MTES and (b) OTES.

$\tilde{\nu}$ (cm ⁻¹)	Vibration	Ceria NPs (%T)	MTES-NPs (%T)	OTES-NPs (%T)
3400	Ce-OH v	0	0	87
2960	CH ₃ v	–	–	84
2920	CH ₂ v _s	–	–	55
2870	CH ₂ v _{as}	–	–	80
1630	Ce-OH v	70	50	86
1460	CH ₃ δ _s	–	–	89
1320	Ce-O-Ce v	85	–	–
1270	Si-CH ₃ v	–	86	79
1120	Si-O-Si v _s	–	84	0
1030	Si-O-Si v _{as}	–	84	26
950	Residual silanol v	–	93	–
780	Ce-O-Si v	–	78	88
720	Ce-O v	60	78	84
530	Ce-O-Si v	–	86	87

Table S2. Transmittance of pristine and SCA-functionalized ceria NPs.

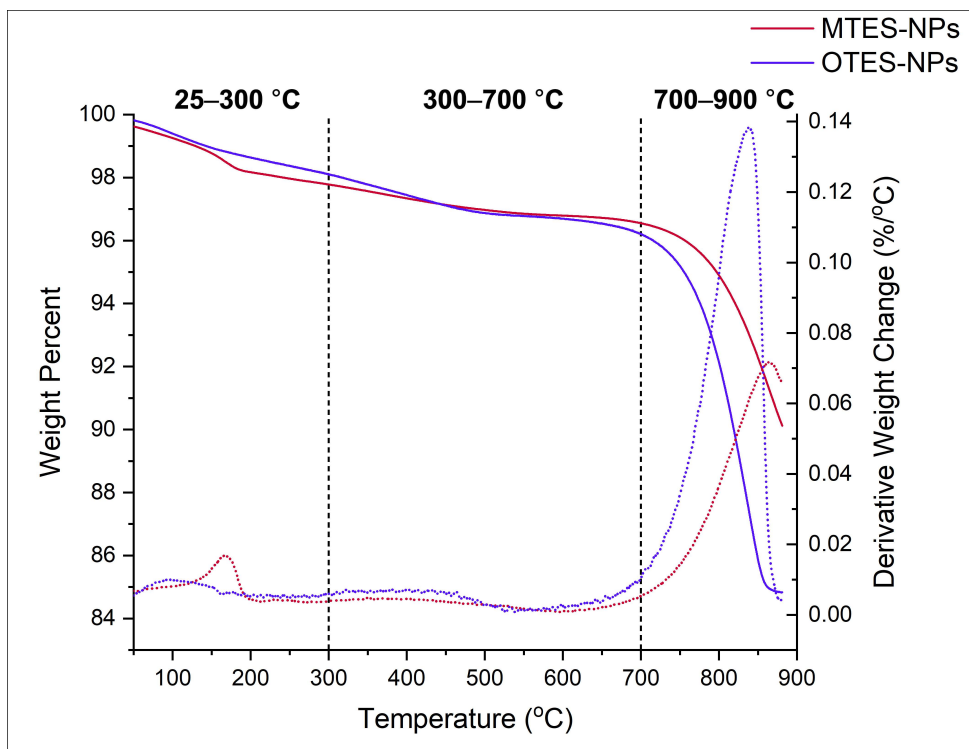


Figure S2. Weight loss and derivative weight change curves for MTES and OTES-NPs given by TGA. No significant difference is observed between the two samples in the lower temperature regimes. The substantial increase in weight loss and derivative weight change in the OTES-NPs above 700 °C is associated with the total decomposition of SCAs, and suggests greater surface loading by OTES-NPs.

<u>Temperature (°C)</u>	<u>Weight Loss Event</u>	<u>MTES-NPs</u>	<u>OTES-NPs</u>
25 – 300	Loss of physisorbed surface water	2.2	1.8
300 – 700	Degradation of silane alkyl chains	1.0	1.4
700 – 900	Decomposition of grafted silanes	6.6	12.0

Table S3. TGA percent weight loss of SCA-functionalized ceria NPs.

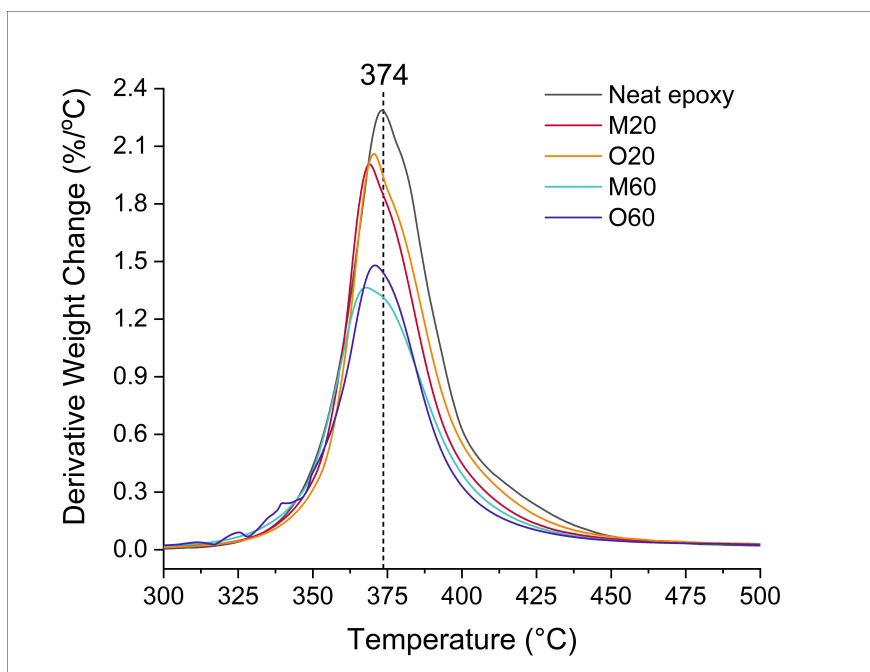


Figure S3. TGA derivative weight loss curves for low and high loading composite samples.

Sample	0 wt%	20 wt%	30 wt%	40 wt%	50 wt%
Neat epoxy	2.25	-	-	-	-
MTES-EPON	-	2.00	1.97	1.67	1.27
OTES-EPON	-	2.05	1.91	1.76	1.47

Table S4. Decomposition rate (%/°C) at derivative weight change T_{\max} of 374 °C.

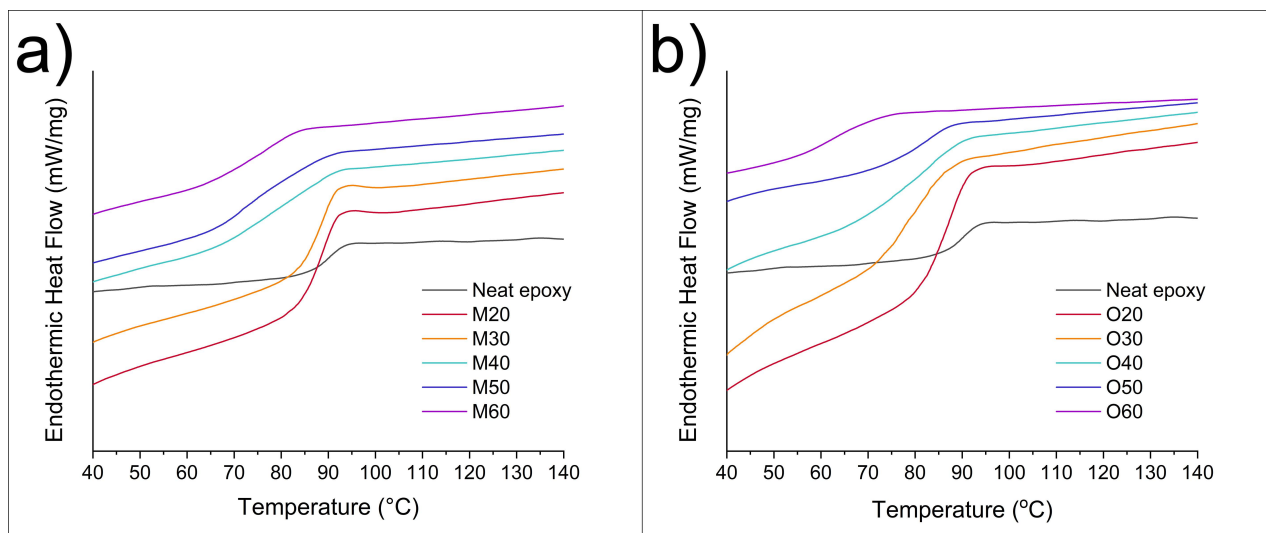


Figure S4. DSC curves used for T_g calculations for all loading values of (a) MTES and (b) OTES composites. DSC thermograms showed a decrease in T_g with increased nanofiller loading for both types of composite.

<u>NP Loading (wt%)</u>	<u>MTES-EPON T_g (°C)</u>	<u>OTES-EPON T_g (°C)</u>
0	90.0	90.0
20	89.0	87.6
30	88.1	86.1
40	79.5	85.3
50	77.8	83.7
60	76.9	83.3

Table S5. Glass transition temperature (T_g) of nanocomposites with different loading levels of SCA-NPs. Values for T_g were determined from the second heating cycle of DSC traces that were collected before samples were irradiated.

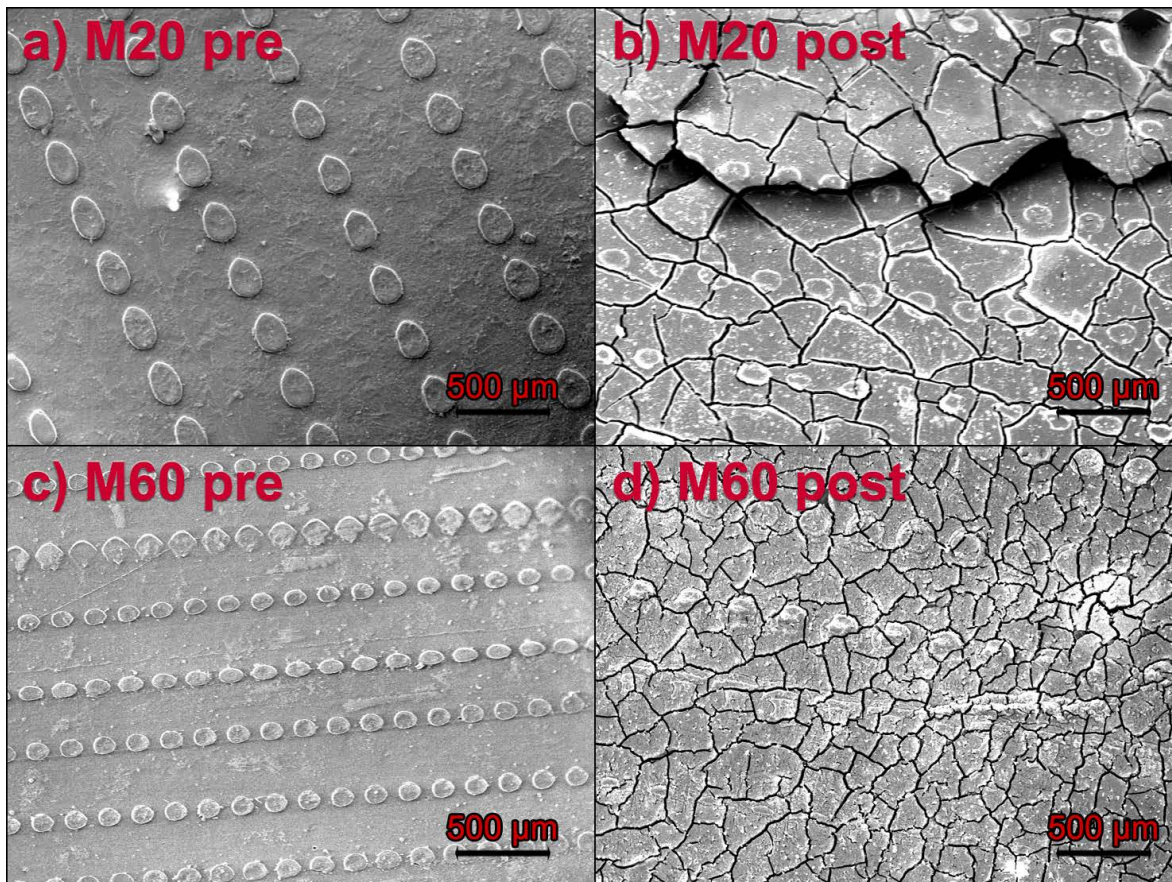


Figure S5. Surface SEM micrographs recorded for M20 and M60 samples recorded before and after heavy ion irradiation.

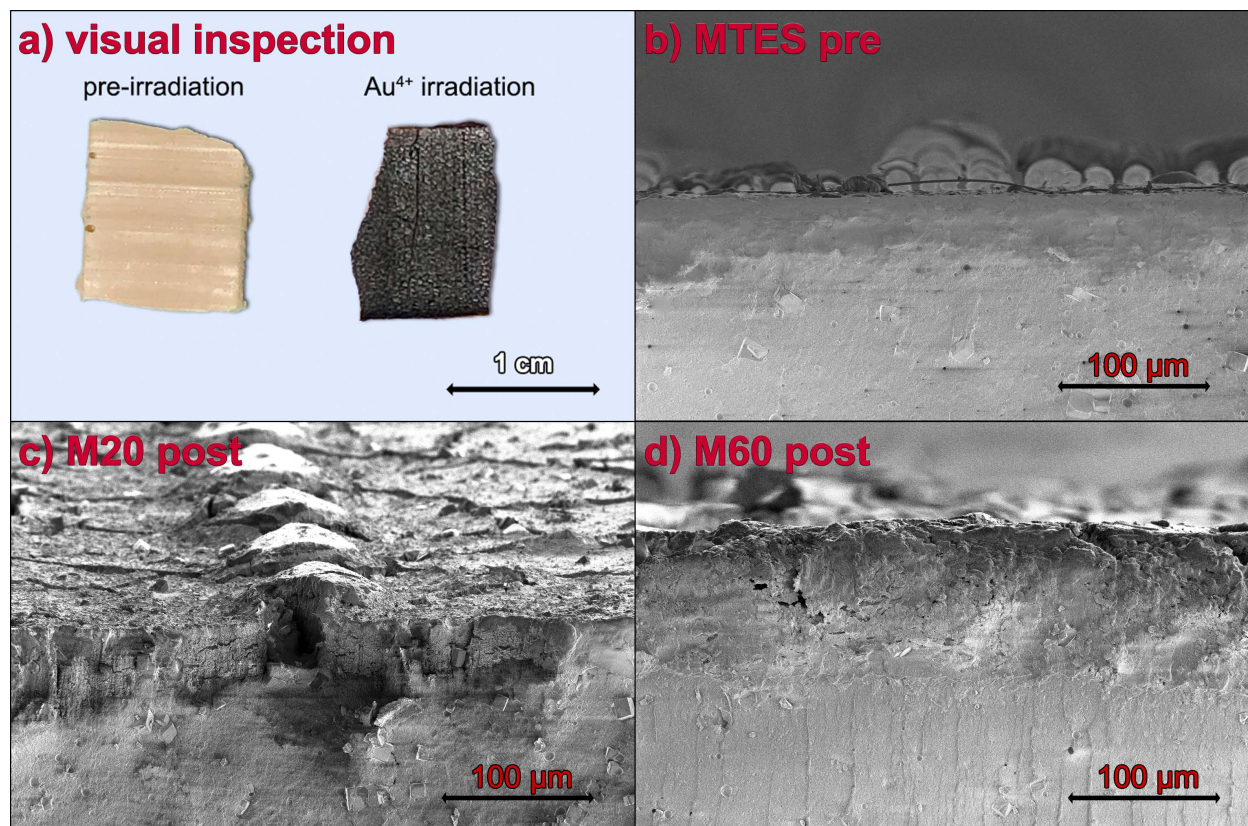
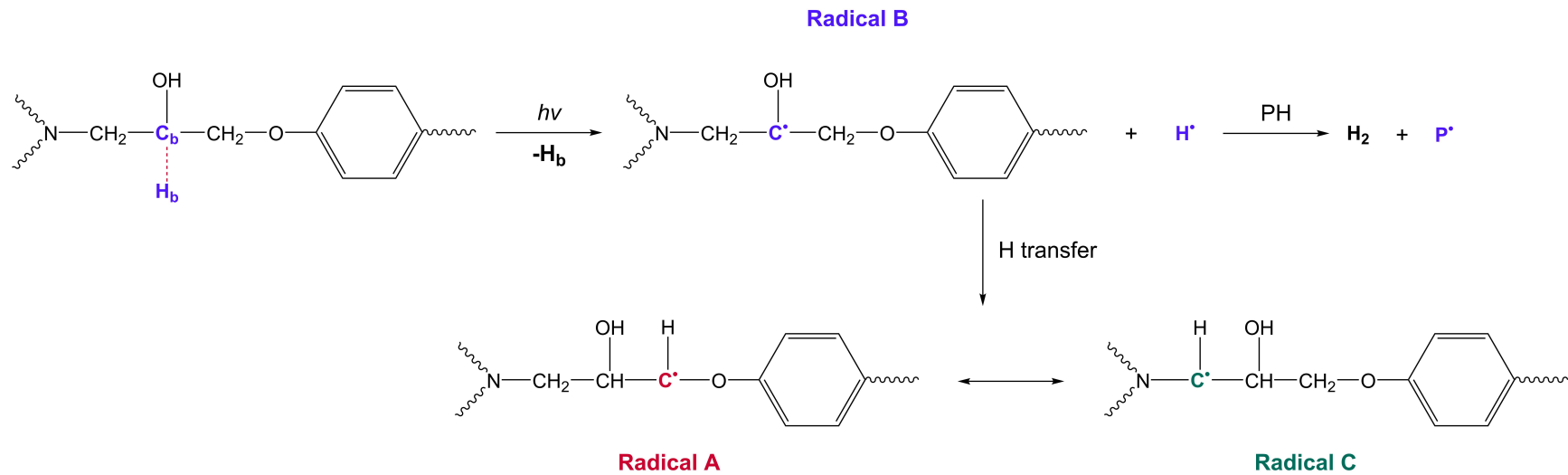
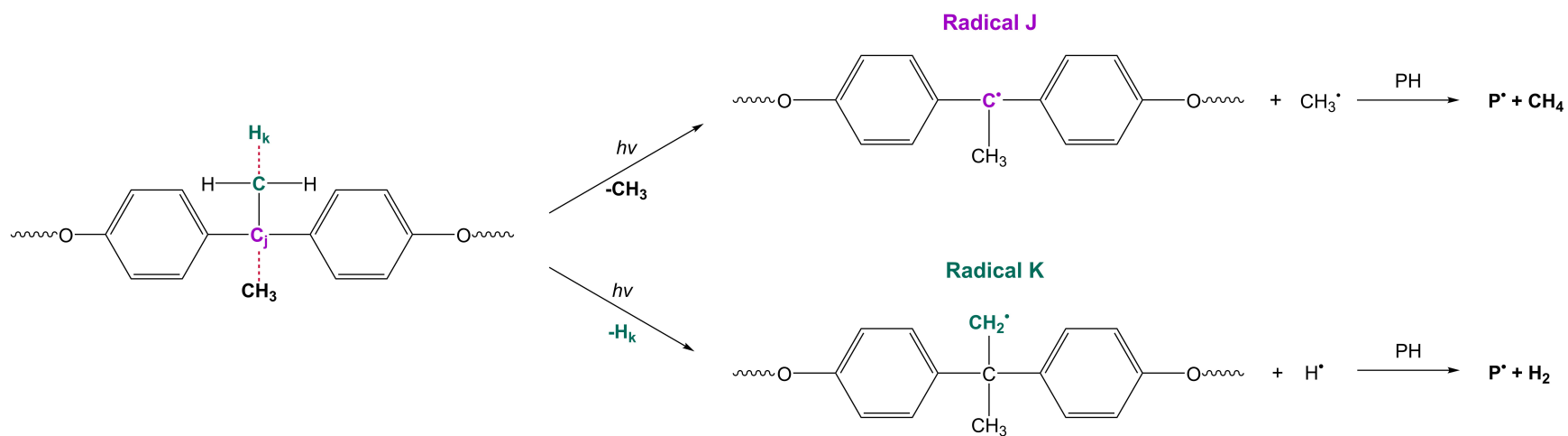


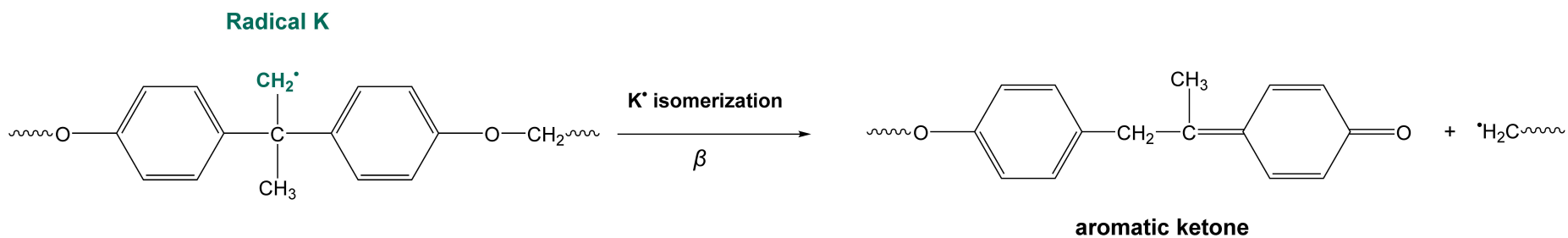
Figure S6. (a) Visual inspection of M60 samples before and after heavy ion irradiation. XSEM images comparing MTES samples before irradiation (b) to irradiated (c) M20 and (d) M60 samples.



Scheme S1. Radiolytic initiation of radical degradation pathways in the epoxy aliphatic segment.



Scheme S2. Radiolytic degradation in bisphenol A moiety initiated by methyl group scission to form Radicals J and K.



Scheme S3. Alternative pathway for bisphenol A moiety degradation initiated by radiolytic hydrogen abstraction from a BPA methyl group to form Radical K, which undergoes isomerization via beta scission to form an aromatic ketone.